IEEE Access
Multidisciplinary | Rapid Review | Open Access Journal

Received 22 April 2024, accepted 13 May 2024, date of publication 16 May 2024, date of current version 28 May 2024.

Digital Object Identifier 10.1109/ACCESS.2024.3402120

RESEARCH ARTICLE

Engineering Ferroelectric HZO With n$^+$-Si/Ge Substrates Achieving High $2P_r = 84\ \mu C/cm^2$ and Endurance > 1E11

ZEFU ZHAO[1], (Graduate Student Member, IEEE), YUN-WEN CHEN[1], YU-RUI CHEN[1], (Graduate Student Member, IEEE), AND C. W. LIU[1,2,3], (Fellow, IEEE)

[1]Graduate Institute of Electronics Engineering, National Taiwan University, Taipei 10617, Taiwan
[2]Graduate Institute of Photonics and Optoelectronics, National Taiwan University, Taipei 10617, Taiwan
[3]Graduate School of Advanced Technology, National Taiwan University, Taipei 10617, Taiwan

Corresponding author: C. W. Liu (cliu@ntu.edu.tw; chee@cc.ee.ntu.edu.tw)

This work was supported in part by the National Science and Technology Council, Taiwan, under Grant NSTC 112-2218-E-002-024-MBK and Grant NSTC 112-2622-8-A49-013-SB; and in part by T-Star Center Project "Future Semiconductor Technology Research Center" under Grant NSTC 113-2634-F-A49-008.

ABSTRACT Metal-Ferroelectric-Metal (MFM) devices possessing high remanent polarizations ($2P_r$) of 84 and 73 $\mu C/cm^2$ are demonstrated with nearly epitaxially grown $Hf_{0.5}Zr_{0.5}O_2$ (HZO) films on (001) n$^+$-Si(3E19/cm^3) and n$^+$-Ge(3E20/cm^3) substrates, respectively, which are higher than MFM devices with HZO films grown on amorphous SiO_2 and partially crystallized TiN underlayers/substrates. The HZO superlattice films by sequential ZrO_2/HfO_2 plasma-enhanced atomic layer deposition (PEALD) process show high crystallinity in TEM images of all devices; however, the measured $2P_r$ values are quite different, ranging from 84 to 33$\mu C/cm^2$. The high-resolution scanning transmission electron microscopy (HR-STEM) images of HZO films on n$^+$-Si and n$^+$-Ge show the polarization axis of o-phase is well-aligned with the growth direction which is consistent with observed high $2P_r$ values. Much lower interfacial energy at o-phase/Si(Ge) interfaces than m-(t-)phase/Si(Ge) by density functional theory (DFT) calculations indicates that o-phase is greatly stabilized in the HZO films on n$^+$-Si(Ge) substrates. Strong $2P_r$ of 51 and 47 $\mu C/cm^2$ are measured after 1E9 and 1E11 endurance cycles for HZO films on n$^+$-Si and n$^+$-Ge substrates, respectively. This study shows epitaxial ferroelectric HZO films could be achieved by using small misfit substrates with the thermal budget as low as 450°C.

INDEX TERMS $Hf_{0.5}Zr_{0.5}O_2$, HZO, epitaxial growth, HR-STEM, PEALD, interfacial energy, density functional theory.

I. INTRODUCTION

Hafnium zirconium oxide ($Hf_{0.5}Zr_{0.5}O_2$, HZO) is an extensively studied material nowadays for its potential applications in ferroelectric RAM (FeRAM), ferroelectric field-effect transistor (FeFET), and ferroelectric tunneling junction (FTJ) due to its great ferroelectricity even under ultrathin condition (∼2nm) [1], and also good scalability plus compatibility with complementary metal-oxide-semiconductor (CMOS) process [2], [3]. To maximize the ferroelectricity, highly crystalized uniform HZO film with its spontaneous polarization along the growth direction is demanded. Because the ferroelectric orthorhombic phase (o-phase) is not the ground state of bulk HZO, using proper substrate with low interfacial energy to stabilize ferroelectric HZO films at the low temperature (∼450°C) is a desired pathway. Previously measured $2P_r$ ranging from 42 to 72$\mu C/cm^2$ [4], [5], [6], [7], [8], [9], [10], [11], [12], [13], [14], [28], [29], [30] is much less than the theoretical values of o-phase [15], [16] probably due to the low content and not well-aligned polarization axis of o-phase among grains in HZO films. Grazing-incidence X-ray diffraction alone could not distinguish between t- and o-phases in ultrathin HZO [17], whereas *P-V* and HR-STEM can confirm the o-phase.

The associate editor coordinating the review of this manuscript and approving it for publication was Shuo Sun.

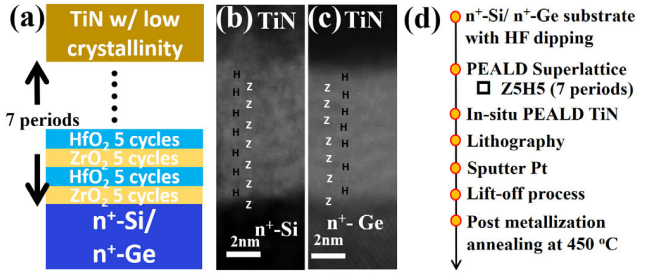

FIGURE 1. (a) Schematic of MFM using n+-Si or n+-Ge substrates with low crystallinity TiN top electrode. The corresponding HAADF images in (b) and (c) clearly show Z(dark)/H(bright) superlattice structures in HZO layers. (d) Process flow of Pt/TiN/$Hf_{0.5}Zr_{0.5}O_2$/n+-Si (n+-Ge).

In this work, nearly epitaxial growth of HZO films on n+-Si and n+-Ge substrates is investigated to improve the content and polarization axis alignment of o-phase in HZO film. It is observed that the measured $2P_r$ values are 84 and 73 $\mu C/cm^2$ for HZO films grown on n+-Si and n+-Ge substrates, respectively, which are much stronger than measured $2P_r$ values for HZO films on α-SiO_2 and TiN underlayers. The Radiant Precision Premier II is used to measure *P-V* with 1kHz. Agilent Technologies B1500A is used to measure endurance with 200ns pulse width. Meanwhile, the polarization axis of HZO films on n+-Si and n+-Ge are also well-aligned along the growth direction as shown in high-resolution STEM (HR-STEM) images, which demonstrates nearly single crystalline o-phase HZO can be epitaxially grown on n+-Si and n+-Ge substrates. The first stacked nanosheet FeFET without amorphous interfacial layer is demonstrated based on this work [21]. Density functional theory (DFT) calculations also reveal that o-phase is highly favored in HZO film grown on Si substrate compared to the monoclinic phase (m-phase) and tetragonal phase (t-phase) to greatly enhance the ferroelectricity of HZO film.

II. DEVICE FABRICATION

In this study, five types of devices are fabricated using different underlayers/substrates namely n+-Si, n+-Ge, α-SiO_2/n+-Si, and *in-situ* TiN with low and high crystallinity. The n+-Si and n+-Ge substrates were used as starting substrates and bottom electrodes after dipping with dilute hydrofluoric acid (DHF) to remove the native oxides. The α-SiO_2/n+-Si substrate was also used to make a comparison of devices with and without DHF dipping treatment. In addition, devices using *in-situ* TiN bottom electrodes prepared by plasma-enhanced atomic layer deposition (PEALD) were also included in comparison to have a better comprehension of the results from the previous three devices. By controlling the TiN thickness, bottom TiN electrodes manifest low (thin) or high (thick) crystallinity. Then HZO superlattice films and *in-situ* TiN top electrodes were deposited by PEALD on five underlayers/substrates with O_2 gas (exposure time of 10 s) and forming gas (50%N_2+50%H_2) at 250°C, respectively. The precursors used for ZrO_2, HfO_2, and TiN are TDMAZ, TEMAH, and TDMAT, respectively. 7 periods (70 cycles) of Z5H5 (ZrO_2 first) PEALD process made of 5 cycles ZrO_2 and 5 cycles HfO_2 were applied for the growth of HZO superlattice film. The Pt passivation layer was sputtered after the TiN deposition on top of HZO to avoid oxidation on top TiN electrode surface and then patterned by the lift-off process. Post metallization annealing (PMA) at 450°C in the forming gas (90% N_2+10%H_2) for 1min was applied to enhance the crystallization in the HZO films during the final process. Fig. 1 (a) shows the schematic of the MFM device using n+-Si or n+-Ge substrate. Fig. 1 (b) and (c) show the high-angle annular dark-field (HAADF) images of devices using n+-Si and n+-Ge substrates, which exhibit clear superlattice structures in HZO films. The HZO superlattice structure was demonstrated to be able to enhance the ferroelectricity of HZO compared to HZO alloy films [1], [5], [17]. In this study, the HZO superlattice structure is applied to all devices. Fig. 1 (d) illustrates the process for fabricating MFM devices.

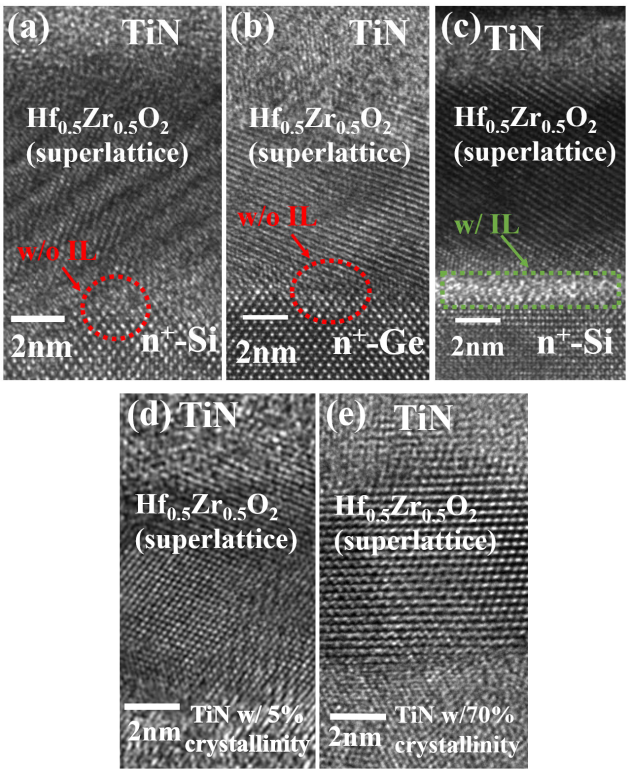

FIGURE 2. TEM of the $Hf_{0.5}Zr_{0.5}O_2$ on (a) n+-Si, (b) n+-Ge, (c) α-SiO_2/n+-Si, (d) 5%, and (e) 70% crystalline TiN underlayer/substrate. No interfacial layer (IL) is observed at (a) HZO/Si and (b) HZO/Ge interface. In (c), α-SiO_2 IL is clear under TEM.

The HZO films in five MFM devices all have high crystallinity as shown in the TEM images of Fig. 2. The moiré fringes presented in the regions of HZO films indicate that HZO films are well crystallized; however, no atomic details could be defined in these TEM images to identify the crystal phase in each HZO film. Compared to devices using n+-Si and n+-Ge substrates, the TEM image of the n+-Si substrate

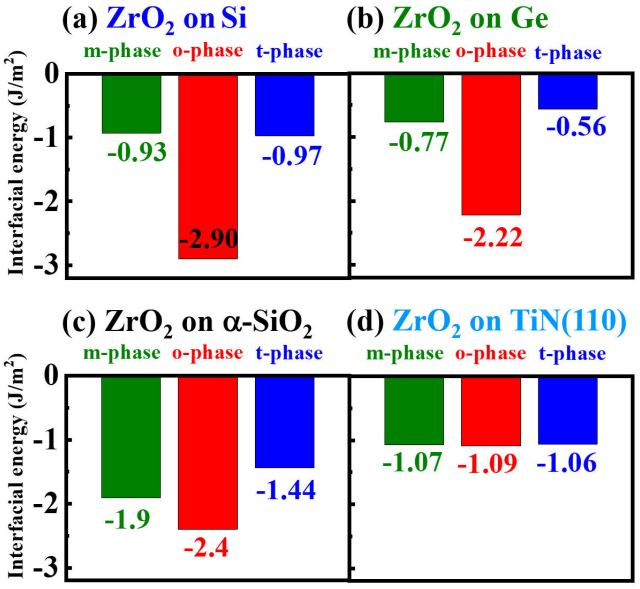

FIGURE 3. Interfacial energies of ZrO_2 phases on (a) Si, (b) Ge, (c) α-SiO_2, and (d) TiN(110) substrate/underlayer by DFT calculations.

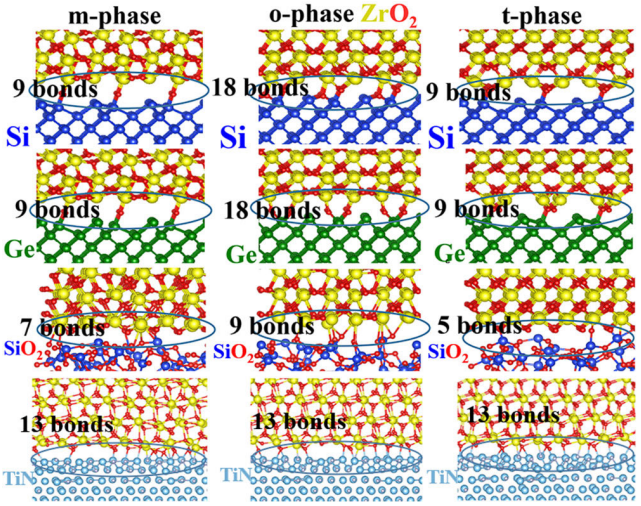

FIGURE 4. Atomic interfaces between ZrO_2 m-, o-, t-phase and underlayers. Larger number of bonds represent lower interfacial energies. Si-O has larger bonding energy than Ge-O.

without DHF dipping treatment has a clear α-SiO_2 interlayer (IL) between the HZO layer and n^+-Si substrate (Fig 2 (c)).

III. SIMULATION

To theoretically understand how the using of different substrates can affect the phase contents in HZO films, atomistic simulations were performed by using Vienna Ab initio Simulation Package (VASP) with density functional theory (DFT) method [18], [19]. The valence electrons of were expanded in plane waves with 500 eV energy cutoff. Electron exchange-correlation energies were estimated based on Perdew–Burke–Ernzerhof generalized gradient approximation (PBE-GGA) functionals. Pseudopotentials constructed

TABLE 1. The lattice constants of o-phase and t-phase for ZrO_2 /HfO_2, Si, Ge, and TiN crystals. The misfits are calculated using the in-plane lattice constants which are defined as $\sqrt{ab}$.

ZrO_2/HfO_2	a (Å)	b (Å)	c (Å)
o-phase	5.32/5.26	5.10/5.04	5.13/5.07
t-phase	5.28/5.20	5.12/5.07	5.12/5.07

	a (Å)	Misfit to o-phase ZrO_2/HfO_2	Misfit to t−phase ZrO_2/HfO_2
Si	5.43	4.2%/5.4%	4.4%/5.7%
Ge	5.66	8.4%/9.9%	8.6%/10.2%
TiN	4.24	-18.6%/-17.7%	-18.5/-17.5%

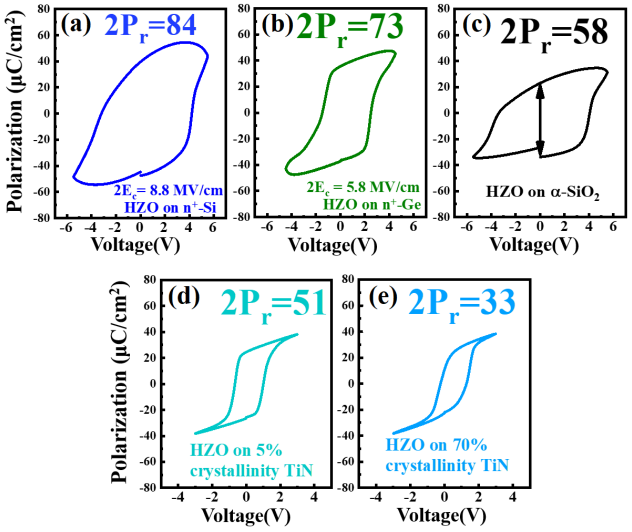

FIGURE 5. The P-V curves of MFM capacitors on (a) n^+-Si, (b) n^+-Ge, (c) α-SiO_2/n^+-Si, and (d) 5% and (e) 70% crystalline TiN substrate.

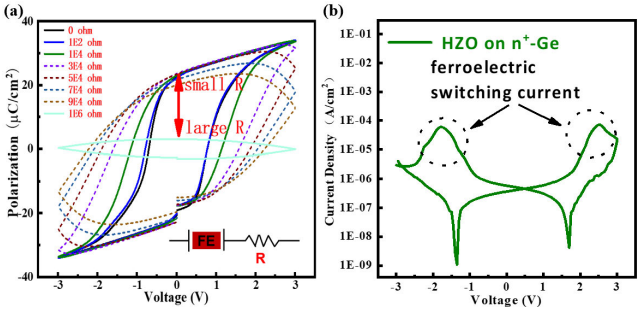

FIGURE 6. (a) The P-V curves of MFM capacitors with additional series connected resistance by Radiant Precision Premier II. (b) The I-V of HZO on n^+-Ge.

by the projected augmented wave method are used to present potential of core electrons. Only Γ point of K-grid was applied for extended simulation systems in calculations of interfacial energies. However, only Si (001), Ge (001), α-SiO_2, and TiN (110) surfaces are considered for the

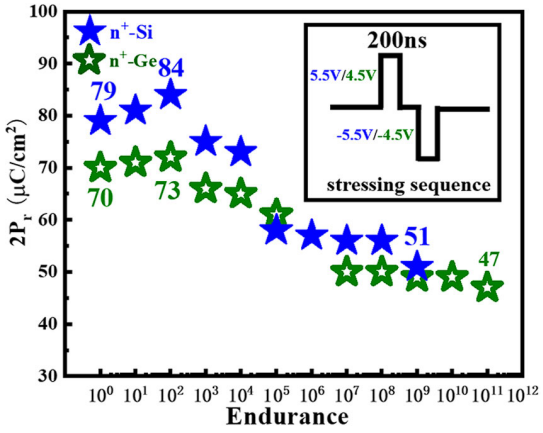

FIGURE 7. Endurance of HZO on n+-Si and n+-Ge with the stressing voltages of ±5.5V and ±4.5V,respectively.

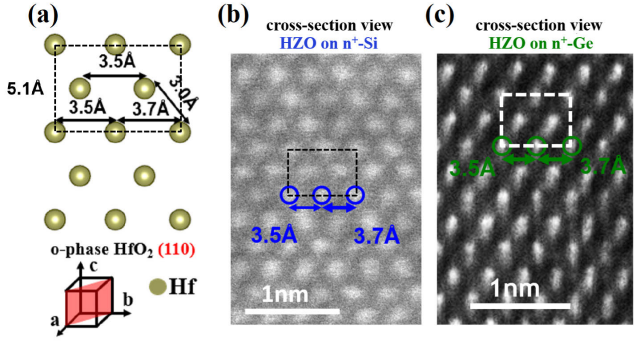

FIGURE 8. (a) The positions of Hf atoms in HfO_2 o-phase in simulation when looking into (110) plane. The HR-STEM images of cross-section view for HZO films grown on n+-Si (b) and n+-Ge (c) substrates.

convenience of computational modeling. The doping in Si and Ge substrates were hence neglected in atomistic models. Since the first deposited layer is ZrO_2 in the PEALD of superlattice HZO film, interfacial energies of ZrO_2 on Si, Ge, α-SiO_2, and TiN were calculated (Fig. 3). For the ZrO_2/Si(Ge) interface, the Si (001) and Ge (001) substrates were constructed with 3 times replicas in two in-plane directions and 8 atomic layers in the z-direction (144 atoms). The ZrO_2 (001) films were constructed with 3 times replicas in two in-plane directions and 4 Zr atomic layers in the z-direction (216 atoms). Since Si and Ge are thick substrates in experiments, the in-plane lattice constants were fixed at Si and Ge lattice constants for modeling ZrO_2/Si(Ge) interfaces. The o-phase formation is stabilized due to much lower interfacial energies of o-phase/Si(Ge) interfaces than m (t-)phase/Si(Ge). The large number of bonds at the interface can represent relative low interfacial energy for the same underlayer (Fig. 4). Note that due to the 3D DFT simulation, not all the bonds can be seen in the 2D plane. The o-phase has twice bonds than the m-(t-)phase on both Si and Ge. Moreover, the o-phase has twice bonds on Si and Ge than on α-SiO_2. The n+-Si has stronger effects on stabilizing the o-phase than n+-Ge due to stronger Si-O bonds.

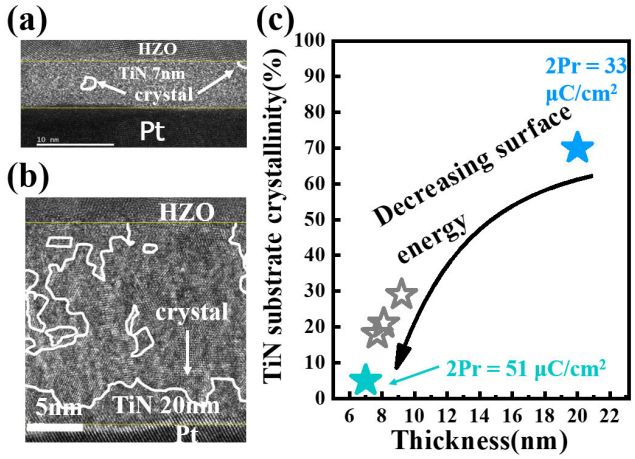

FIGURE 9. TEM images of (a) thinner (7nm) and (b) thicker (20nm) TiN substrates. (c) Crystallinity of TiN decreases with thickness due to decreasing surface energy.

IV. RESULT AND DISCUSSION

The *P-V* curves of five MFM devices are shown in Fig. 5. The measured $2P_r$ values are 84, 73, 58, 51, and 33μC/cm^2 for HZO films grown on n+-Si, n+-Ge, α-SiO_2/n+-Si, and *in-situ* TiN with low and high crystallinity at room temperature, respectively. The high $2P_r$ confirms the HZO o-phase. However, these measured $2P_r$ values are all smaller than the theoretical values of HZO o-phase ranging from 100 to 136 μC/cm^2 [15], [16]. Compared to the *P-V* curves of MFM devices using TiN substrates, the *P-V* curves of devices using n+-Si, n+-Ge and α-SiO_2/n+-Si substrates are more rounded may be because of the additional series connected resistance caused by the low doping in n+-Si and n+-Ge substrates. The coercive voltages of MFM capacitors increase with increasing resistance (Fig. 6 (a)). The ferroelectric switching current of HZO on n+-Ge is clear (Fig. 6 (b)).

Since the HZO o-phase is generally recognized as the source of ferroelectricity in HZO film [20], [21], [22], to reach the theoretical $2P_r$ value needs very high o-phase content in HZO film and also well-aligned polarization axis with the growth direction, that is the normal of underlayer/substrate. According to the measured $2P_r$, using n+-Si substrate seems the best one to enhance HZO o-phase content and to make the HZO o-phase polarization axis along the growth direction.

To achieve good alignment of the polarization axis, the HZO film better near epitaxially grows on the substrate. Hence low misfit between HZO o-phase and underlayer/substrate should be one of the important factors to be addressed. Among Si, Ge, and TiN cubic phases, the Si crystal has the smallest misfit with ZrO_2 o-phase, next Ge, and then TiN as shown in Table 1. On the other hand, the misfits of Si and Ge with ZrO_2 t-phase are slightly larger than with ZrO_2 o-phase, which would result in the o-phase is more favored than the t-phase for HZO film on n+-Si and n+-Ge substrates.

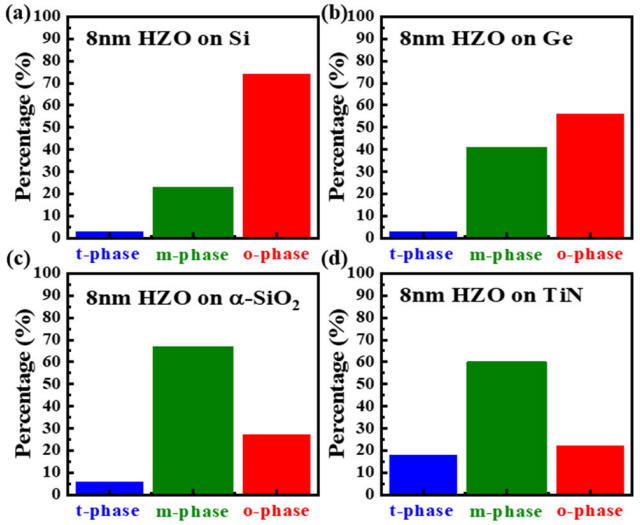

FIGURE 10. Phase percentage estimation of HZO film grown on (a) Si, (b) Ge, (c) α-SiO_2, and (d) TiN (110) underlayer/substrate at temperature of 450°C with [Vo] = 1%.

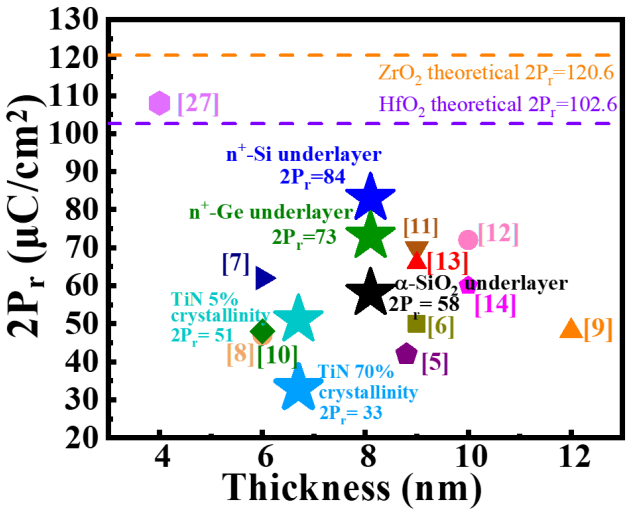

FIGURE 11. Benchmarks of $2P_r$. HZO with n^+-Si substrate shows a record high $2P_r$ of 84μC/cm^2.

Because oxides naturally grow on Si and Ge wafers under ambient conditions, DHF dipping treatment was applied to remove oxides before the HZO superlattice PEALD process for the first two MFM devices to ensure the clean crystalline surface of n^+-Si and n^+-Ge substrates. These two devices show pretty large $2P_r$ values of 84 and 73μC/cm^2. In addition, after 1E9 and 1E11 endurance cycles, still strong $2P_r$ of 51 and 47 μC/cm^2 are measured, respectively (Fig.7). The $2P_r$ increases for the first ~100 cycles may be due to the wake-up effect [31]. On the other hand, with an additional interfacial α-SiO_2 layer, HZO film grown on α-SiO_2/n^+-Si substrate has smaller $2P_r$ value of 58μC/cm^2 compared to HZO on n^+-Si and n^+-Ge substrates (Fig. 5(a)-(c)).

Recently, S. S. Cheema et al. showed that HZO superlattice grown on α-SiO_2/Si substrate exhibits strong ferroelectricity even down to 2nm HZO thickness [1]. According to our previous theoretical study, the amorphous underlayer like α-SiO_2 can enhance the o-phase content for lower interfacial energy than m-phase and t-phase [23]. However, the not uniform surface of α-SiO_2 also increases the variation of different crystal orientations among HZO grains to result in not uniform alignments of the polarization axis and reduce measured $2P_r$.

To confirm the o-phase and alignments of the polarization axis in HZO films on n^+-Si and n^+-Ge substrates, the HR-STEM images of HZO films in cross-section view (growth direction pointing up) of these two devices are compared with the simulated Hf positions in HfO_2 o-phase crystal looking into (110) plane as shown in Fig. 8. The polarization axis is along o-phase c-axis. Since HR-STEM is more sensitive to heavy atoms like Hf and Zr, the white spots in Fig. 8 (b) and (c) present the positions of Hf or Zr atoms while O atoms are not visible. The HR-STEM images in Fig. 8 (b) and (c) exhibit high similarity with the simulated o-phase Hf positions in Fig. 8 (a), which indicate the crystalline o-phase in HZO films grown on n^+-Si and n^+-Ge substrates. Meanwhile, these HR-STEM images also provide clear evidence that the polarization axis of o-phase in HZO films on n^+-Si and n^+-Ge substrates are well aligned.

With respected to the MFM devices using TiN substrates, the measured $2P_r$ values are all smaller than those of the previous three devices. In addition, HZO film grown on the TiN substrate with 70% high crystallinity has a lower $2P_r$ value than the HZO film grown on the TiN substrate with much lower 5% crystallinity (Fig. 5 (d) and (e)). To be noted, the crystallinity of a TiN substrate is calculated by counting the crystalline area in the TEM images of TiN substrates (Fig. 9 (a) and (b)). The crystallinity of TiN substrate will decrease with decreasing thickness for the decreasing surface energy [25]. For TiN substrates, the interface with higher amorphous conditions shows a higher $2P_r$ value due to the large lattice misfit between HZO o-phase and cubic TiN.

Based on our experimental results, it is intuitively clear that when the misfit between o-phase and substrate is small, the epitaxial growth of HZO film is likely to happen with greatly enhanced crystallinity and well alignment of polarization axis of HZO film. On the other hand, if the misfit between the o-phase and substrate is large, the amorphous interface condition could reduce the incompatibility between HZO phases and the crystalline grains in the substrate. The o-phase content could be enhanced if the o-phase is more stabilized by the interfacial energy at the amorphous interface while the alignment of the polarization axis between grains will not be assured.

According to the calculated interfacial energies (Fig. 3), ZrO_2 o-phase is more stabilized on Si, Ge, α-SiO_2, and TiN (110) underlayers/substrates relative to m-phase and t-phase for lower interfacial energies. However, the relative differences among interfacial energies of three ZrO_2

phases are not similar for different underlayers/substrates. Si substrate has the largest differences, Ge substrate is next, then α-SiO_2 underlayer, and then TiN (110) substrate has the smallest differences. The calculated interfacial energies indicate that Si substrate possesses the greatest ability to stabilize ZrO_2 o-phase among four theoretically modeled underlayers/substrates.

In experiments, the HZO films usually are polycrystalline with grain size roughly proportional to the HZO film thickness [26]. To estimate the o-phase content in HZO films grown on different underlayers/substrates with respected to HZO thickness, the phase percentages are calculated at 450 °C. Fig. 10 presents the estimation of phase percentage with 8nm HZO thickness. For HZO film on Si and Ge substrate, the content of o-phase is much higher than t- and m-phase (Fig. 10 (a) and (b)). Both Si and Ge substrates can have very high o-phase content at very thin conditions because of extremely suppressed m-phase and t-phase contents. On the other hand, HZO o-phase content is not the major phase on α-SiO_2 and TiN underlayer (Fig. 10 (c) and (d)). It is because the m- and t-phase is not extremely suppressed for HZO on the TiN and α-SiO_2 underlayer.

Fig. 11 shows the benchmarks of $2P_r$ values observed in this work and several previous works. If the o-phase is 100% percentage with well-aligned c-axis, the $2P_r$ will reach the theoretical value. Ultra-high polarization of 108 $\mu C/cm^2$ in nanometer-scaled size (95 nm × 85 nm) was observed by F. Huang et al. by using Mo electrodes [27], which meets the theoretical $2P_r$ values of bulk HfO_2 and ZrO_2 indicated by the purple and orange dashed lines in Fig. 9 (102.6 and 120.6 $\mu C/cm^2$, respectively, by our calculations). The ultra-high $2P_r$ measured by F. Huang et al. resulted from a single o-phase grain in a very thin HZO film with a very small area size. Except for that special record, others were measured with device sizes larger than 1 μm^2 and are all smaller than the theoretical $2P_r$ values. The largest $2P_r$ value is 84 $\mu C/cm^2$ for MFM using n^+-Si substrate in this work. The factor like polycrystalline nature of HZO film could be the main reason for the smaller $2P_r$ measured in this work compared to theoretical values, since the alignments of the polarization axis are well parallel to the growth direction as demonstrated in HR-TEM (Fig. 8).

By simply using the theoretical average $2P_r$ ($111.6\mu C/cm^2$) could convert the o-phase content in Fig. 11 to $2P_r$ value at different HZO thickness for different underlayers/substrates. The predicted o-phase content is 74% for HZO on Si substrate at HZO thickness of 8nm, which corresponds to a $2P_r$ value, 82.6 $\mu C/cm^2$, very close to the experimental value in this work. For HZO on Ge substrate, the predicted o-phase content and $2P_r$ are 55% and 61.4 $\mu C/cm^2$ which are also not too far from the experimental value in this work. For HZO on α-SiO_2 underlayer, the predicted o-phase content and $2P_r$ are 27% and 30.1 $\mu C/cm^2$ which are smaller than the experimental observation. For HZO on TiN(110) substrate, the predicted o-phase content and $2P_r$ are 24% and 26.7 $\mu C/cm^2$ which are smaller than the experimental value by using low crystallinity TiN substrate but close to the data by using high crystallinity TiN substrate. In general, the theoretical predictions of models using crystalline substrates are close to our experimental data, but the result of using an amorphous underlayer like α-SiO_2 is underestimated. The not well-matched results for the case of HZO on α-SiO_2 underlayer are reasonable since our α-SiO_2 slab model could not fully represent the ergodic surface conditions of true α-SiO_2 surface. After all, the trend of theoretical prediction is still consistent with the experimental observation in this work.

V. CONCLUSION

The strategy to grow single crystalline ferroelectric HZO film is demonstrated by the nearly epitaxial growth of o-phase HZO on small misfit Si and Ge substrates. The measured $2P_r$ values of the corresponding MFM devices reach high records of 84 and 73 $\mu C/cm^2$, respectively. The corresponding HR-TEM images clearly manifest the polarization axis of these two HZO films are well aligned with growth direction. Theoretical calculations show Si and Ge substrates greatly favor the HZO o-phase compared to α-SiO_2 underlayer and TiN substrate.

ACKNOWLEDGMENT

An earlier version of this paper was presented in part at the IEEE Symposium on VLSI Technology and Circuits (VLSI Technology and Circuits), Kyoto, Japan, June 2023 [DOI: 10.23919VLSITechnologyandCir57934.2023.10185233].

REFERENCES

[1] S. S. Cheema, N. Shanker, L. C. Wang, C. H. Hsu, S. L. Hsu, Y. H. Liao, M. S. Jose, J. Gomez, W. Chakraborty, W. Li, and J. H. Bae, "Ultrathin ferroic HfO_2–ZrO_2 superlattice gate stack for advanced transistors," *Nature*, vol. 604, no. 7904, pp. 65–71, Apr. 2022, doi: 10.1038/s41586-022-04425-6.

[2] M. H. Park, Y. H. Lee, H. J. Kim, Y. J. Kim, T. Moon, K. D. Kim, J. Müller, A. Kersch, U. Schroeder, T. Mikolajick, and C. S. Hwang, "Ferroelectricity and antiferroelectricity of doped thin HfO_2-based films," *Adv. Mater.*, vol. 27, no. 11, pp. 1811–1831, Mar. 2015, doi: 10.1002/adma.201404531.

[3] W. Banerjee, A. Kashir, and S. Kamba, "Hafnium oxide (HfO_2)—A multifunctional oxide: A review on the prospect and challenges of hafnium oxide in resistive switching and ferroelectric memories," *Small*, vol. 18, no. 23, May 2022, Art. no. 2107575, doi: 10.1002/smll.202107575.

[4] Y.-R. Chen, Z. Zhao, C.-T. Tu, Y.-C. Liu, B.-W. Huang, Y. Xing, G.-H. Chen, and C. W. Liu, "ION enhancement of $Ge_{0.98}Si_{0.02}$ nanowire nFETs by high-k dielectrics," *IEEE Electron Device Lett.*, vol. 43, no. 10, pp. 1601–1604, Oct. 2022, doi: 10.1109/LED.2022.3201972.

[5] M. H. Park, H. J. Kim, G. Lee, J. Park, Y. H. Lee, Y. J. Kim, T. Moon, K. D. Kim, S. D. Hyun, H. W. Park, H. J. Chang, J.-H. Choi, and C. S. Hwang, "A comprehensive study on the mechanism of ferroelectric phase formation in Hafnia–Zirconia nanolaminates and superlattices," *Appl. Phys. Rev.*, vol. 6, no. 4, Nov. 2019, Art. no. 041403, doi: 10.1063/1.5118737.

[6] T.-Y. Wu, H.-H. Huang, Y.-H. Chu, C.-C. Chang, M.-H. Wu, C.-H. Hsu, C.-T. Wu, M.-C. Wu, W.-W. Wu, T.-S. Chang, H.-Y. Lee, S.-S. Sheu, W.-C. Lo, and T.-H. Hou, "Sub-nA low-current HZO ferroelectric tunnel junction for high-performance and accurate deep learning acceleration," in *IEDM Tech. Dig.*, San Francisco, CA, USA, Dec. 2019, pp=. 6, doi: 10.1109/IEDM19573.2019.8993565.

[7] Y. Goh, J. Hwang, Y. Lee, M. Kim, and S. Jeon, "Ultra-thin $Hf_{0.5}Zr_{0.5}O_2$ thin-film-based ferroelectric tunnel junction via stress induced crystallization," *Appl. Phys. Lett.*, vol. 117, no. 24, Dec. 2020, Art. no. 242901, doi: 10.1063/5.0029516.

[8] Y.-F. Chen, L.-W. Hsu, C.-W. Hu, G.-T. Lai, and Y.-H. Wu, "Enhanced tunneling electro-resistance ratio for ferroelectric tunnel junctions by engineering metal work function," *IEEE Electron Device Lett.*, vol. 43, no. 2, pp. 208–211, Feb. 2022, doi: 10.1109/LED.2021.3133577.

[9] Y. Liu, Y. Cao, H. Zhu, L. Ji, L. Chen, Q. Sun, and D. W. Zhang, "$HfZrO_2$-based ferroelectric tunnel junction with crested symmetric band structure engineering," *IEEE Electron Device Lett.*, vol. 42, no. 9, pp. 1311–1314, Sep. 2021, doi: 10.1109/LED.2021.3102226.

[10] J. Hwang, Y. Goh, and S. Jeon, "Effect of forming gas high-pressure annealing on metal-ferroelectric-semiconductor Hafnia ferroelectric tunnel junction," *IEEE Electron Device Lett.*, vol. 41, no. 8, pp. 1193–1196, Aug. 2020, doi: 10.1109/LED.2020.3001639.

[11] S.-J. Chang, C.-Y. Teng, Y.-J. Lin, T.-M. Wu, M.-H. Lee, B.-H. Lin, M.-T. Tang, T.-S. Wu, C. Hu, E. Y.-T. Tang, and Y.-C. Tseng, "Visualizing ferroelectric uniformity of $Hf_{1-x}Zr_xO_2$ films using X-ray mapping," *ACS Appl. Mater. Interfaces*, vol. 13, no. 24, pp. 29212–29221, Jun. 2021, doi: 10.1021/acsami.1c08265.

[12] Y.-D. Lin, P.-C. Yeh, Y.-T. Tang, J.-W. Su, H.-Y. Yang, Y.-H. Chen, C.-P. Lin, P.-S. Yeh, J.-C. Chen, P.-J. Tzeng, M-H. Lee, T.-H. Hou, S.-S. Sheu, W.-C. Lo, and C.-I. Wu, "Improving edge dead domain and endurance in scaled $HfZrO_x$ FeRAM," in *IEDM Tech. Dig.*, San Francisco, CA, USA, 2021, p. 6, doi: 10.1109/IEDM19574.2021.9720692.

[13] M. I. Popovici, J. Bizindavyi, P. Favia, S. Clima, M. N. K. Alam, R. K. Ramachandran, A. M. Walke, U. Celano, A. Leonhardt, S. Mukherjee, O. Richard, A. Illiberi, M. Givens, R. Delhougne, J. Van Houdt, and G. S. Kar, "High performance la-doped HZO based ferroelectric capacitors by interfacial engineering," in *IEDM Tech. Dig.*, San Francisco, CA, USA, Dec. 2022, p. 6, doi: 10.1109/IEDM45625.2022.10019525.

[14] T. Fu, M. Zeng, S. Liu, H. Liu, R. Huang, and Y. Wu, "Record-high $2P_r$=60 $\mu C/cm^2$ by sub-5ns switching pulse in ferroelectric lanthanum-doped HfO_2 with large single grain of orthorhombic phase >38 nm," in *IEDM Tech. Dig.*, San Francisco, CA, USA, Dec. 2022, p. 6, doi: 10.1109/IEDM45625.2022.10019386.

[15] S. V. Barabash, D. Pramanik, Y. Zhai, B. Magyari-Kope, and Y. Nishi, "Ferroelectric switching pathways and energetics in $(Hf,Zr)O_2$," *ECS Trans.*, vol. 75, no. 32, pp. 107–121, Jan. 2017, doi: 10.1149/07532.0107ecst.

[16] R. Materlik, C. Künneth, and A. Kersch, "The origin of ferroelectricity in $Hf_{1-x}Zr_xO_2$: A computational investigation and a surface energy model," *J. Appl. Phys.*, vol. 117, no. 13, Apr. 2015, Art. no. 134109, doi: 10.1063/1.4916707.

[17] Z. Zhao, Y.-R. Chen, J.-F. Wang, Y.-W. Chen, J.-R. Zou, Y. Lin, Y. Xing, C. W. Liu, and C. Hu, "Engineering $Hf_{0.5}Zr_{0.5}O_2$ ferroelectric/antiferroelectric phases with oxygen vacancy and interface energy achieving high remanent polarization and dielectric constants," *IEEE Electron Device Lett.*, vol. 43, no. 4, pp. 553–556, Apr. 2022, doi: 10.1109/LED.2022.3149309.

[18] G. Kresse and J. Furthmüller, "Efficient iterative schemes for ab initio total-energy calculations using a plane-wave basis set," *Phys. Rev. B, Condens. Matter*, vol. 54, no. 16, pp. 11169–11186, Oct. 1996, doi: 10.1103/physrevb.54.11169.

[19] G. Kresse and J. Furthmüller, "Efficiency of ab-initio total energy calculations for metals and semiconductors using a plane-wave basis set," *Comput. Mater. Sci.*, vol. 6, no. 1, pp. 15–50, Jul. 1996, doi: 10.1016/0927-0256(96)00008-0.

[20] Z. Zhao, Y.-R. Chen, Y.-W. Chen, J.-F. Wang, Y. Xing, W. Ji, G.-H. Chen, J.-Y. Lee, R. Dobhal, and C. W. Liu, "Engineering $Hf_{0.5}Zr_{0.5}O_2$ ferroelectric tunnel junctions with amorphous WO_x bottom electrodes achieving high remanent polarization and record low-operating voltage," *IEEE Trans. Electron Devices*, vol. 70, no. 10, pp. 5022–5027, Oct. 2023, doi: 10.1109/TED.2023.3308924.

[21] Y.-R. Chen, Y.-C. Liu, Z. Zhao, W.-H. Hsieh, J.-Y. Lee, C.-T. Tu, B.-W. Huang, J.-F. Wang, S.-J. Chueh, Y. Xing, G.-H. Chen, H.-C. Chou, D. S. Woo, M. H. Lee, and C. W. Liu, "First stacked nanosheet FeFET featuring memory window of 1.8 V at record low write voltage of 2 V and endurance >1E11 cycles," in *Proc. IEEE Symp. VLSI Technol. Circuits (VLSI Technol. Circuits)*, Jun. 2023, pp. 1–2, doi: 10.23919/vlsitechnologyandcir57934.2023.10185284.

[22] Y. Xing, Y.-R. Chen, J.-F. Wang, Z. Zhao, Y.-W. Chen, G.-H. Chen, Y. Lin, R. Dobhal, and C. W. Liu, "Improved ferroelectricity in cryogenic phase transition of $Hf_{0.5}Zr_{0.5}O_2$," *IEEE J. Electron Devices Soc.*, vol. 10, pp. 996–1002, 2022, doi: 10.1109/JEDS.2022.3218004.

[23] Y.-W. Chen and C. W. Liu, "Boost of orthorhombic population with amorphous SiO_2 interfacial layer—A DFT study," *Semiconductor Sci. Technol.*, vol. 37, no. 5, Mar. 2022, Art. no. 05LT01, doi: 10.1088/1361-6641/ac5a5e.

[24] Z. Zhao, Y.-R. Chen, Y.-W. Chen, W.-H. Hsieh, J.-F. Wang, J.-Y. Lee, Y. Xing, G.-H. Chen, and C. W. Liu, "Towards epitaxial ferroelectric HZO on n^+-Si/Ge substrates achieving record $2Pr = 84$ $\mu C/cm^2$ and endurance >1E11," in *Proc. IEEE Symp. VLSI Technol. Circuits (VLSI Technol. Circuits)*, Kyoto, Japan, Jun. 2023, pp. 1–2, doi: 10.23919/vlsitechnologyandcir57934.2023.10185233.

[25] S. H. N. Lim, D. G. McCulloch, M. M. M. Bilek, and D. R. McKenzie, "Relation between microstructure and stress in titanium nitride films grown by plasma immersion ion implantation," *J. Appl. Phys.*, vol. 93, no. 7, pp. 4283–4288, Apr. 2003, doi: 10.1063/1.1558995.

[26] M. H. Park, Y. H. Lee, H. J. Kim, T. Schenk, W. Lee, K. D. Kim, F. P. G. Fengler, T. Mikolajick, U. Schroeder, and C. S. Hwang, "Surface and grain boundary energy as the key enabler of ferroelectricity in nanoscale Hafnia–Zirconia: A comparison of model and experiment," *Nanoscale*, vol. 9, no. 28, pp. 9973–9986, Jun. 2017, doi: 10.1039/c7nr02121f.

[27] F. Huang, B. Saini, L. Wan, H. Lu, X. He, S. Qin, W. Tsai, A. Gruverman, A. C. Meng, H.-S.-P. Wong, P. C. McIntyre, and S. S. Wong, "First observation of ultra-high polarization (~108 $\mu C/cm^2$) in nanometer scaled high performance ferroelectric HZO capacitors with Mo electrodes," in *Proc. IEEE Symp. VLSI Technol. Circuits (VLSI Technol. Circuits)*, Kyoto, Japan, Jun. 2023, pp. 1–2, doi: 10.23919/vlsitechnologyandcir57934.2023.10185240.

[28] W. Zhang, G. Li, X. Long, L. Cui, M. Tang, Y. Xiao, S. Yan, Y. Li, and W. Zhao, "A comparative study of the X-ray radiation effect on Zr-doped and Al-doped HfO_2-based ferroelectric memory," *Phys. Status Solidi (B)*, vol. 257, no. 5, May 2020, Art. no. 1900736, doi: 10.1002/pssb.201900736.

[29] Y. Mao, W. Zhang, L. Cui, M. Tang, P. Su, X. Long, G. Li, Y. Xiao, and S. Yan, "Growth kinetics of the ferroelectric al-doped HfO_2 thin films via synergistic effect of various essential factors," *Ceram. Int.*, vol. 47, no. 4, pp. 4674–4680, Feb. 2021, doi: 10.1016/j.ceramint.2020.10.034.

[30] W. L. Zhang, Y. H. Mao, L. Cui, M. H. Tang, P. Y. Su, X. J. Long, Y. G. Xiao, and S. A. Yan, "Impact of the radiation effect on the energy storage density and wake-up behaviors of antiferroelectric-like Al-doped HfO_2 thin films," *Phys. Chem. Chem. Phys.*, vol. 22, no. 38, pp. 21893–21899, 2020, doi: 10.1039/d0cp04196c.

[31] A. M. Walke, M. I. Popovici, K. Banerjee, S. Clima, P. Kumbhare, J. Desmet, J. Meersschaut, G. V. D. Bosch, R. Delhougne, G. S. Kar, and J. V. Houdt, "Electrical investigation of wake-up in high endurance fatigue-free La and Y doped HZO metal–ferroelectric–metal capacitors," *IEEE Trans. Electron Devices*, vol. 69, no. 8, pp. 4744–4749, Aug. 2022, doi: 10.1109/TED.2022.3186869.

ZEFU ZHAO (Graduate Student Member, IEEE) received the B.S. degree in optoelectronics from the School of Optics and Photonics, Beijing Institute of Technology, in 2018. He is currently pursuing the Ph.D. degree with the Graduate Institute of Electronics Engineering, National Taiwan University, Taipei, Taiwan.

His research interests include ferroelectric HZO superlattice, epitaxial HZO, MFM capacitors, antiferroelectric HZO alloy, FeRAM, FTJ, stacked nanosheet GAAFeFETs, and high-k capacitors.

YUN-WEN CHEN is currently a Postdoctoral Researcher with the Prof. C. W. Liu's Group, National Taiwan University, Taiwan. His expertise is in atomistic modeling via density functional theory and molecular dynamics simulations with force fields. His current research interests include ferroelectricity in HZO thin films and complex functional oxides applying in semiconductors and energy harvesting.

YU-RUI CHEN (Graduate Student Member, IEEE) is currently pursuing the Ph.D. degree with the Graduate Institute of Electronics Engineering, National Taiwan University, Taipei, Taiwan.

His current research interests include multi-level nanosheet GAAFeFETs, stacked nanosheet GAAFeFETs, ferroelectric HZO superlattice, stacked nanowire/nanosheet GAAFETs with high-k integrated, and multi-Vt modulation of dipole-controlled work function metal.

C. W. LIU (Fellow, IEEE) received the B.S. and M.S. degrees in electronics engineering from National Taiwan University, Taipei, Taiwan, in 1985 and 1987, respectively, and the Ph.D. degree in electrical engineering from Princeton University, Princeton, NJ, USA, in 1994.

From 2002 to 2005, he was the Research Director with the Industrial Technology Research Institute, Hsinchu, Taiwan. From 2008 to 2013, he was the Deputy General Director with National Nano Device Laboratories, Hsinchu. He is currently a Distinguished Professor with the Department of Electrical Engineering, National Taiwan University. He has more than 704 articles (more than 271 journal articles, 32 IEDM, and 18 VLSI), 76 U.S. patents, two China patents, 50 Taiwan patents, more than 8692 citations with an H-index of 43, 44 Ph.D. graduates, and 143 master's graduates. His research interests include SiGe/GeSn epi/photonics, stacked 3D transistors for beyond 1 nm nodes, thermal analysis of 3DIC, IGZO TFT, SRAM/MIM/FTJ/FeFET/MTJ/SOT/DRAM, and CMOS image sensors.